J Mater Sci (2010) 45:3912–3920
DOI 10.1007/s10853-010-4451-2

Comparative study on characteristics of hybrid laser-TIG welded AZ61/Q235 lap joints with and without interlayers

Xiao-dong Qi · Li-ming Liu

Received: 27 December 2009 / Accepted: 27 March 2010 / Published online: 13 April 2010

Abstract AZ61 Mg alloy to Q235 mild steel were lap joined using hybrid laser-TIG welding technique. At the joint interface and fusion zone (FZ), microstructure was revealed by scanning electron microscopy equipped with energy dispersive X-ray spectroscopy; element distribution was analyzed by electron probe micro-analyzer; intermediate phases were identified using X-ray diffraction test. Comparing with interlayer-free joints, the new intermediate phases Mg_2Ni and Mg_2Cu were generated in the FZ and at the Mg alloy/interlayer interface, and the solid solution of Ni or Cu in Fe was found along the edge of weld pool on steel side. It was found that direct joint without any interlayer was mechanical bonding, while Ni- and Cu-added joints were semi-metallurgical bonding. The joint shear strength was not only related to the penetration depth, but also related to the bonding mode. The strengthening effect on Cu-added joint was higher than that on Ni-added joint.

Introduction

Magnesium alloys with their unique properties such as lower density, excellent electromagnetic interference shielding, and damping capability have extensive applying potential [1]. Although many components of Mg alloy can be processed using casting and extruding methods [2], the manufacture of some complex components may not be done without welding techniques. So far, Mg alloys especially Mg–Al–Zn alloys have been welded with many techniques such as tungsten inert gas (TIG) welding [3–6], laser-beam welding (LBW) [7–9], electron-beam welding (EBW) [1, 10], friction stir welding (FSW) [11, 12], and brazing [13], etc. The demands for dissimilar materials' welding are increasing in industry.

At present, it is no doubt that steel is still one of the dominant materials used in industry. Joining Mg alloys and steel together is challengeable owing to great difference in physical and chemical properties. From the Mg–Fe diagram, it can be seen that no intersolubility and intermediate phases between Mg and Fe elements could be found. Chen and Nakata [14] studied that the joining mechanism of friction stir welded joint between AZ31 Mg alloy and steel was mechanical bonding. Wielage et al. [15] reported that no element diffusion process occurred at AZ31 Mg alloy/steel interface by soldering technique. Our previous work [16, 17] investigated that the bonding mode of AZ31B Mg alloy to steel without any interlayer was mechanical, while it was metallurgical after the addition of intermediate elements into the joint. Cu and Ni are widely used elements for improving the weld properties such as toughness, ductility, and strength [18, 19]. Both Cu and Ni can react with Mg and Fe in terms of their binary diagrams, thus metallurgical bonding between AZ61 Mg alloy and Q235 mild steel may be realized, which may contribute to the improvement of joint strength. The welding of these two materials with Cu and Ni interlayers may also provide guidance for future welding between Mg alloy and stainless steel or Ni-based steel [20]. In addition, the joining of two materials together may also protect people from electromagnetic radiation especially applying to the electronic products.

However, the joining of AZ61 Mg alloy to steel with Cu and Ni intermediate elements has not been reported. Thus

X. Qi · L. Liu (✉)
Institute of Welding Technology, Schools of Materials Science and Engineering, Dalian University of Technology, Dalian 116024, China
e-mail: Liulm@dlut.edu.cn

the present paper mainly concentrated on the characteristics comparison of microstructure and tensile properties of lap joint between the two materials with and without Cu and Ni interlayers.

Experimental procedure

The materials used in the experiment are a 2 mm thick AZ61 Mg alloy sheet and a 1.2 mm thick Q235 mild steel sheet, which were cut into 60 × 80 mm, and the composition of them is shown in Table 1. It can be seen from Table 1 that Q235 steel is equivalent to the Cr.D steel of AST-USA or E235B of 630-ISO. Before welding these sheets were degreased and ground by acetone and abrasive cloth. Ni and Cu interlayers employed are both 0.1 mm thick and 99.9% purity.

The experimental setup and the workpiece are shown in Fig. 1a. Nd:YAG pulsed laser equipped with TIG welding machine was employed in the welding process which is called hybrid laser-TIG welding technique. Lap joint configuration with an overlapping width of 10–15 mm was adopted shown in Fig. 1a and the Mg alloy was placed on the steel sheet. The acute angle between laser beam and TIG torch is 50° with the axis of laser-beam perpendicular to the workpiece surface. When the interlayers were used, they were set between the Mg alloy and steel shown in Fig. 1a. The welding parameters in the experiment are shown in Table 2 which maintain invariant, and laser energy used is shown in Table 3. Laser is a leading role during welding as the penetration depth inside steel depends mainly on laser energy. Laser is generated by excitation current; therefore, the variation of current against time was employed in the experiment, the regime of which is shown in Fig. 1c and the total duration of laser is 2.8 ms for the single pulse shape.

Table 2 Welding parameters of laser and TIG

Pulsed frequency, Hz	30
Defocus, mm	−3
TIG current (AC), A	75
Argon gas flow rate, L/min	TIG: 12, Laser: 5
Welding speed, mm/min	750
Acute angle, α	50°

Table 3 Laser energy used in the experiment

	Laser energy, W
A	360–370
B	380–400
C	410–420
D	430–450

Table 1 Composition of AZ61 Mg alloy and Q235 mild steel

	Element, wt%								
	Mg	Al	Zn	Si	Mn	P	S	C	Fe
AZ61	Bal.	5.5–7.5	0.5–1.5	≤0.018	0.15–0.4	–	–	–	≤0.01
Q235	–			0.12–0.30	0.30–0.65	≤0.045	0.050	0.14–0.22	Bal.

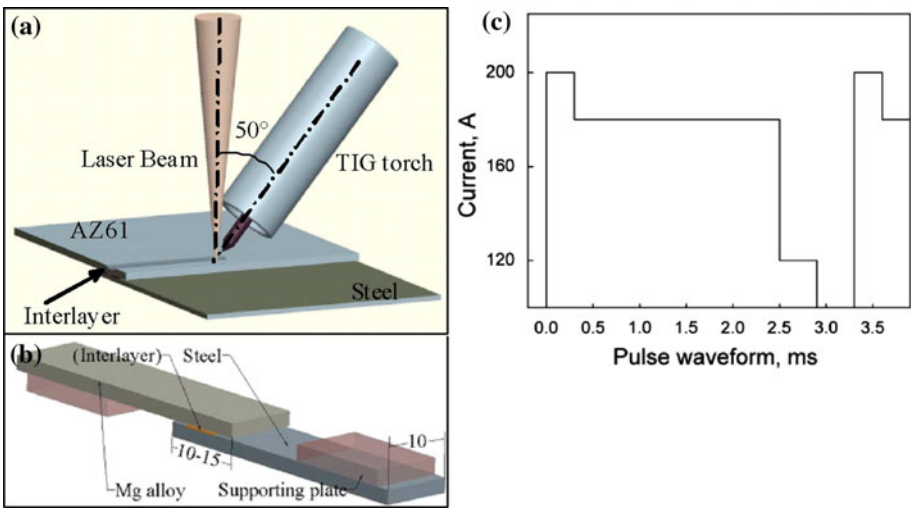

Fig. 1 Sketch of experimental setup (**a**), shear test specimen (**b**), and the pulse laser regime (**c**), (mm)

After welding, tensile specimens were cut from the workpiece shown in Fig. 1b. Supporting plates were added to the ends of the specimen to maintain the joint interface parallel to the load direction. The shear strength was calculated by following the equation

$$\sigma_{b\_shear} = \frac{F}{S_{\parallel}} \quad (1)$$

where F and σ_{b_shear} are the load and the tensile shear strength, respectively; $S_{\parallel}$ is a rectangular contact area at the Mg alloy/steel interface parallel to the load direction, which could also be evaluated according to the size of fracture surface shown in Fig. 10a–c. Tensile shear test was conducted by electronic universal testing machine Css-2205 with a travel speed of 2 mm/min at room temperature. The value of shear strength is the average of at least three specimens.

Transverse sections of the specimens were etched by Nital's reagent (vol. 4% HNO_3 ethanol solution) for 10–15 s. Microstructures were examined by scanning electron microscopy (SEM) equipped with energy dispersive X-ray spectroscopy (EDS) analysis system, element distribution at the joint interface was performed with electron probe micro-analyzer (EPMA), and the intermediate phase in the fusion zone (FZ) was also identified by X-ray diffraction (XRD) test. Vickers microhardness was also carried out in the FZ with 200 gf and dwell time of 15 s.

Results

Relationships among laser power, penetration depth, and joint shear strength

Figure 2a shows that the penetration depth increases with the augment of laser power, indicating that the depth mainly depends on the laser power under the condition of maintaining other welding parameters constant during welding. However, the joint shear strength does not increase invariantly with enhancement of the depth shown in Fig. 2b, but reaches maximum shear strength and then decreases swiftly. Accordingly, the maximum strength for each sort of joint must correspond to a penetration depth value, and thus an optimum laser power which is approximately 420 W is also attained. In addition, it could also be seen from Fig. 2 that the penetration depth of direct joints is higher than that of interlayer-added joints, whereas the shear strength of direct joints is much lower than that of interlayer-added joints.

Microstructures of different joints

Direct joint

The transverse sections of different joint are shown in Fig. 3. As some spatters were generated in the welding process, some big particles were likely to exist in weld pool. The particles which are mainly steel in Fig. 3a and b are bigger than that in other images. While part of the particulates in Fig. 3c and d are composed of Fe and Ni elements, and those in Cu-added joints of Fig. 3e and f contain Cu element according to EDS analysis. Distinct boundaries exist in between Mg alloy and steel shown in Fig. 3.

The line analysis in Fig. 4e indicates that there is no diffusion process occurred at the Mg alloy/steel interfaces. Due to large difference in the hardness of the two materials, the cross-sections of Mg alloy and steel are not in the same level seen in Fig. 4a–c, in addition, gaps indicated by arrows could be seen in Fig. 4b. As heat input of the arc is much greater, and due to a large cooling rate during welding, the melt of Mg alloy in FZ would be solidified swiftly, and thus the grains of Mg alloy of the FZ could be refined (see Fig. 3d). The white dots which are mainly distributed dispersively in the FZ contain (wt) 36.2% Al, 58.4% Mg, and 5.4% O according to the EDS analysis, suggesting that they are the second phase β-$Mg_{17}Al_{12}$ that is consistent with the results in Ref. [21]. Due to a fast

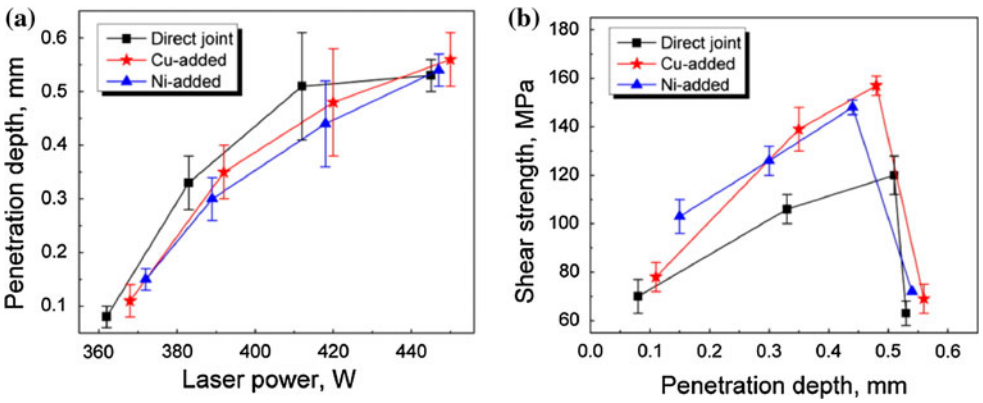

Fig. 2 Correlation between penetration depth and laser power (**a**), and between shear strength and penetration depth (**b**) of different joints

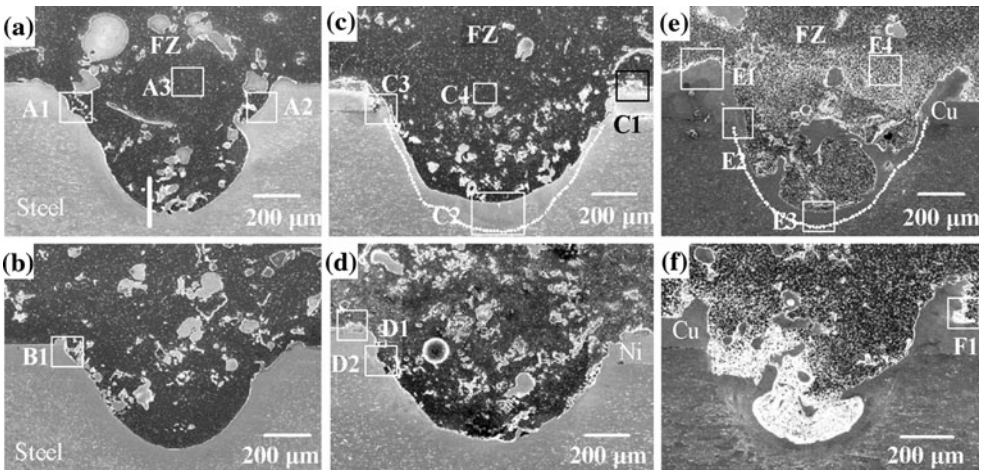

Fig. 3 SEM images of cross-sectioned weld joints: **a**, **b** are direct joints; **c**, **d** are Ni-added joints; **e**, **f** are Cu-added joints. **a**, **c**, **e** were obtained at optimum laser power, while **b**, **d**, **f** were done at 380–390 W of laser power

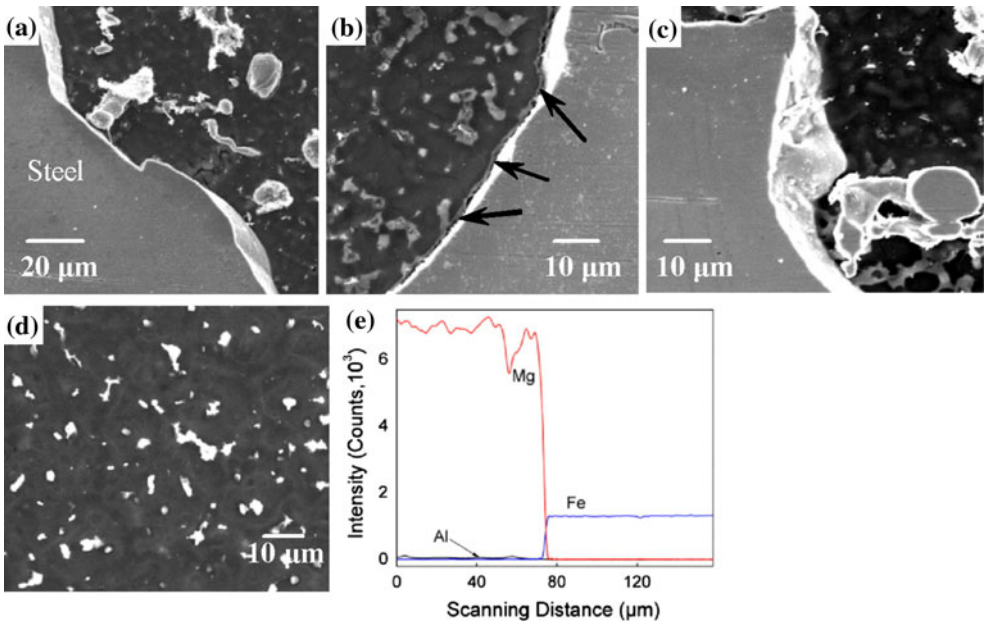

Fig. 4 Microstructures of the direct joint and line analysis: **a**, **b**, **d**, **c** from region A1, A2, A3, and B1 of Fig. 3a and b, respectively, **e** line analysis along the line at the *bottom* of the pool in Fig. 3a

cooling process, a supersaturated solid solution of Al in Mg was formed and would precipitate extra Al element to construct β-phase in the solidifying process.

Ni-added joints

Figure 3c and d are the joints with Ni interlayer. There are also some particles inside the FZ, from which the difference is that some of them are composed of Ni element. It is noteworthy that a transitional zone (TZ) is produced between the dotted line and the boundary in Fig. 3c. In order to investigate the composition of the TZ, line analysis was carried out along the line at the bottom shown in Fig. 5b, and the results are in Fig. 6b. It can be seen that Fe and Ni elements are included in the TZ, which is the solid solution of Ni in Fe according to Fe–Ni binary diagrams. Such result is consistent with the composition analysis that is (wt) 18.3% Ni with the rest of Fe according to EDS test. In the welding process, the steel and Ni interlayer in the welding pool must be melted at the same time and dissolved into each other, whereas the mixture of them could still be maintained without decomposition due to swift solidifying in the welding process. However, when the mixture of Ni and Fe was in liquid state, its temperature

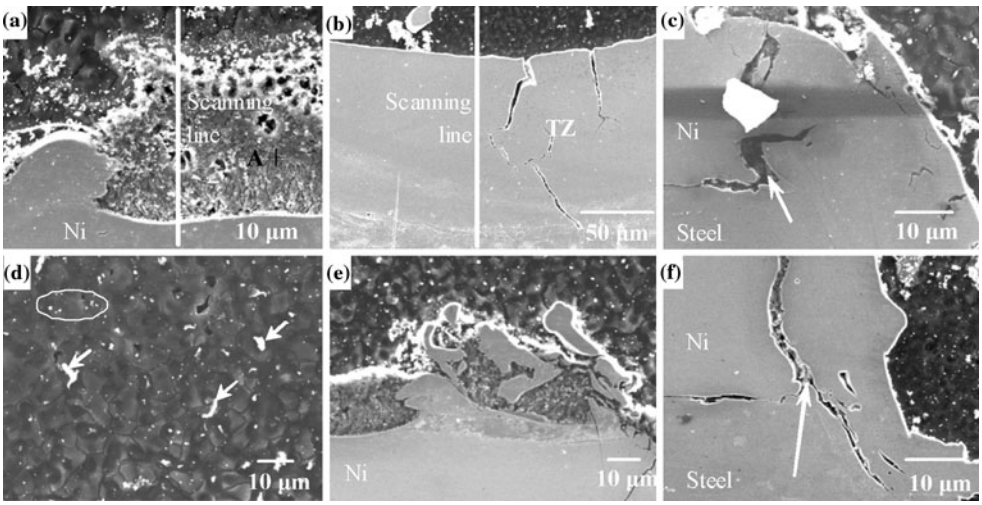

Fig. 5 Microstructures of the Ni-added joints: **a**–**d** from the region C1, C2, C3, and C4 in Fig. 3c, respectively, **e**, **f** from D1 and D2 in Fig. 3d, respectively

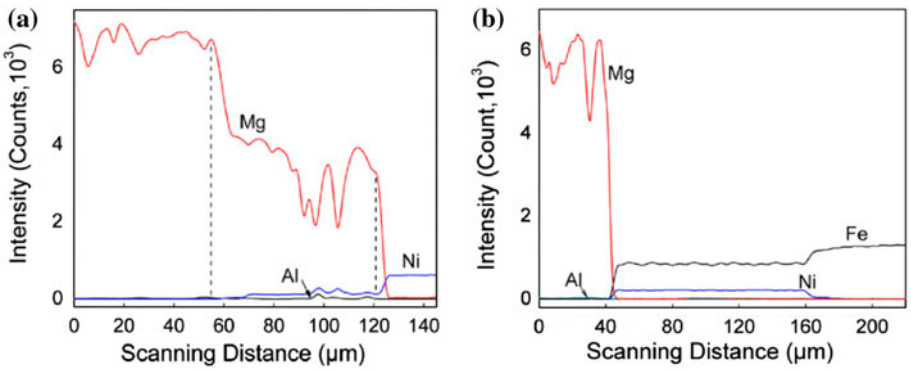

Fig. 6 Elements distribution at the interfaces: **a** from the scanning line in Fig. 5a, **b** from Fig. 5b

must be as high as 1400 °C at which Mg element must be in gaseous state. Therefore, there is no chance for Mg and Ni to be reacted at the same time, and thus no intermetallic compound (IMC) layer was found in the pool. Nonetheless, the Mg alloy plate was mainly melted by the arc of TIG torch in the welding process, and the thermal energy provided by the arc for the reaction of Mg and Ni was sufficient, consequently, a layer of IMC was generated on Ni interlayer adjacent to the upper edge of the pool shown in Fig. 5a and e. While line scanning was performed at the Mg/Ni interface in Fig. 5a, and the results between the dashed line in Fig. 6a shows that Mg and Ni elements are included into the IMC layer at the interface. EDS results show that point A of Fig. 5a contains (wt) 40.1% Mg and 59.9% Ni implying that the IMC layer is composed of Mg_2Ni which is also proved by the XRD results of Fig. 7a.

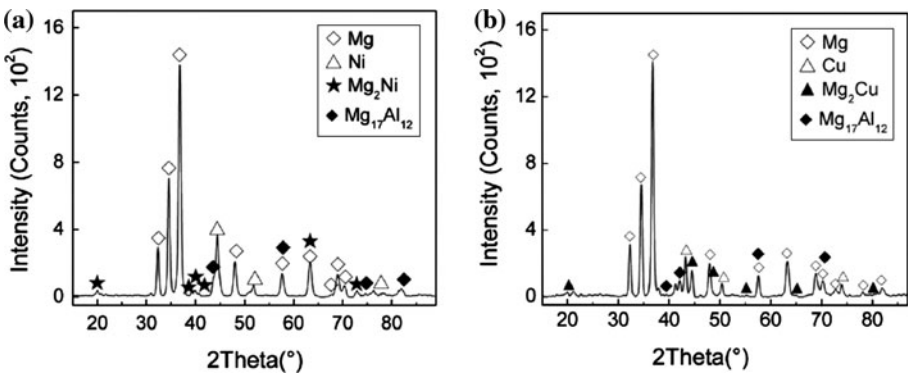

Fig. 7 Phase species in the FZ: **a** Ni-added joints, **b** Cu-added joints

In addition, the variation of Al element in Fig. 6a shows that no interaction occurred between Al and Ni, but could be the inclusion of the second phase $Mg_{17}Al_{12}$ into the IMC layer, which is also verified further by XRD analysis shown in Fig. 7a. Figure 5c and f exhibit similar bonding mode between Ni and steel. And a bad bonding location pointed by an arrow in respective Fig. 5c and f is likely to be where the stress concentration occurred during tensile shear test, which has been verified, as Fig. 10b shows that all the interlayers are attached to the Mg alloy tightly, implying that the fracture did took place between the interlayer and steel.

It could be found from Fig. 5d that equiaxed grains of the FZ are even finer than that of direct joint shown in Fig. 4d. The white dots pointed by arrows are still $Mg_{17}Al_{12}$ phase which distributed inside crystals according to EDS analysis. And the smaller white dots circled in elliptical region in Fig. 5d contain Ni element according to the results of EDS, suggesting that they are the Mg_2Ni intermetallic phases which have been confirmed by XRD analysis of Fig. 7a.

Cu-added joints

The microstructure of Cu-added joints is shown in Fig. 3e and f. It seems that a vortex pattern took place in the pool before those big particles were generated. Probably, these particles were the result of a drastic flow of the melt in the pool. A TZ between the dotted line and the boundary could also be seen along the edge of the pool without cracks on it. Fig. 8b shows that the remelted Cu intermixed well with the steel. Line analysis was performed at the bottom of the pool in Fig. 8c and the results in Fig. 9b suggest that only few Cu elements with approximate (wt) 3% according to EDS analysis in point A of Fig. 8c dissolved into Fe, which implies that the TZ was constructed by limited solid solution of Cu in Fe. In addition, the variation of Al curve in Fig. 9b indicates that Al element interacted only with Mg elements. The case of the TZ production in Cu-added joint is almost the same as that in Ni-added joint, the difference of which is that the limited solid solution of Cu in Fe was generated in the TZ. As the Fe–Cu binary diagram tells us that no IMC but solid solution is generated between

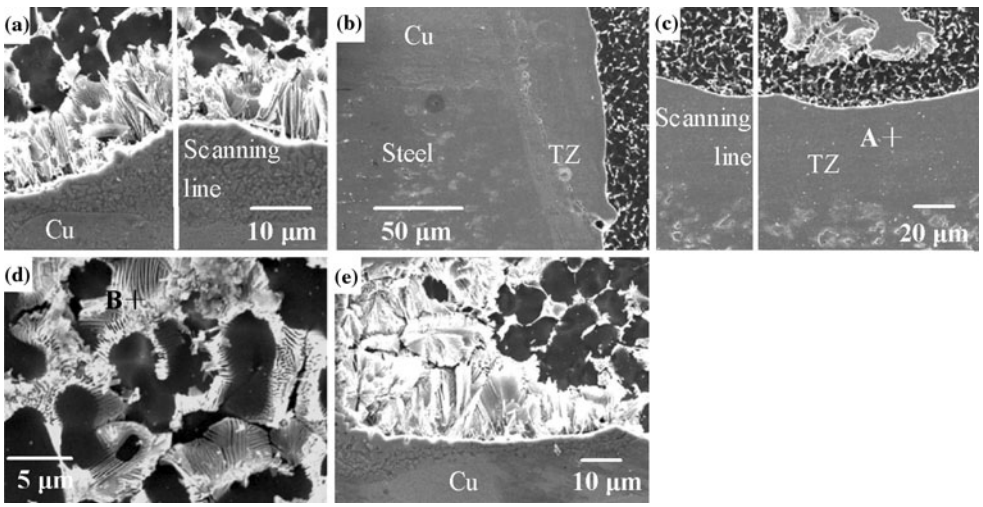

Fig. 8 Microstructures of the Cu-added joints: **a**–**e** from E1, E2, E3, E4, and F1 in Fig. 3e and f, respectively

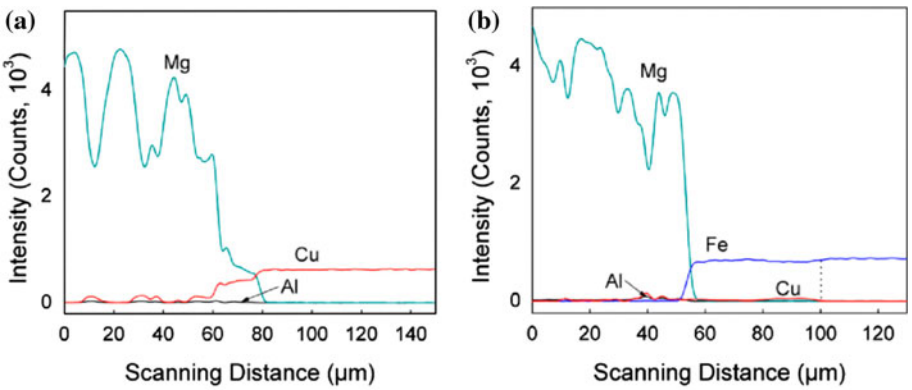

Fig. 9 Elements distribution at the interfaces: **a** from the scanning line in Fig. 8a, **b** from Fig. 8c

the two elements. Thus most of Cu elements that were not dissolved into steel got plenty of chances to interact with Mg elements; accordingly, large numbers of second phases were formed in the FZ (see Fig. 2e, f). Figure 8d shows the delicate structure of the second phase whose composition is (wt) 49.3% Mg and 50.7% Cu according to the EDS results in point B. It could be inferred that the phase is Mg_2Cu, which is also testified by the XRD results in Fig. 7b. However, the Mg_2Cu phase with discontinuous reticular structure constituted hypereutectic structure with the remelted Mg alloy in the FZ. Besides, the new phase did not only disperse uniformly in the FZ, but also grew from top of Cu interlayer (see Fig. 7a).

Line analysis shown in Fig. 9a indicates that there are two layers at the Mg/Cu interface which could also be seen in Fig. 8a and e. The white layer contains (wt) 52.1% Mg, 45.9% Cu, and 5.5% Al, implying that it is the mixture of Mg_2Cu and $Mg_{17}Al_{12}$ phases which is coincided with the results in Fig. 7b. It can be seen that the layer displays loosen lamella structure on Cu interlayer. The darker layer underneath that IMC layer is mainly consisted of small particles whose composition is (wt) 88.2% Cu, 7.8% Mg, and 4% Al according to the EDS analysis, implying that the dark layer is mainly composed of remelted Cu with some solute of Mg and Al.

Shear strength of different joints

The results of tensile shear test are shown in Fig. 10. It is such narrow bonding area with average 1 mm width that joins the sheets of AZ61 Mg alloy with Q235 mild steel shown in Fig. 10a, b, and c. The narrow weld seam on steel surface could only be attributed to the action of laser in the welding process, because the width of laser beam is much smaller than that of arc in present experiment. The interlayers of Ni and Cu were all attached to Mg alloy tightly after tensile shear test, indicating that an effective joining between Mg alloy and Ni or Cu interlayer was obtained; meanwhile it also suggests that the IMCs of Mg_2Ni and Mg_2Cu played a crucial role in the welding process.

Figure 10d is the result of tensile shear strength of all types of joints which corresponds to that in Fig. 3. 145 MPa is nominal ultimate tensile shear strength (UTSS) of base material AZ61 Mg alloy. In comparison with Fig. 3, it could be seen that the shear strength is not only closely related to the penetration, but also correlated intimately to the bonding mode of the joint, which will be discussed later. The role of the interlayers is vital in elevating the joint shear strength from direct joints to those with interlayers.

Fracture surface after tensile test

The addition of Ni and Cu interlayer to the joints enhanced the joint shear strength significantly, which could also be seen from morphology of the joint fracture surface shown in Fig. 11. Figure 11a is the fracture mode of direct joint and Fig. 11b is that of the interlayer-added joint. There are clear boundaries between smooth and rough areas shown in Fig. 11c. And the smooth surface is much wider than the rough area with lots of dimples shown in the magnified image. Intergranular facets and the arrises which are even as long as the width of the weld pool could be seen on the fracture surface of direct joints. The rough areas are actually the fractured Mg alloy in the FZ with good plasticity, thus they are presented with many dimples. As there is no interaction at Mg alloy/steel interface according to the line analysis of Fig. 4e, most fracture locations are completely brittle shown in Fig. 11c. When Ni or Cu interlayers were added into the joints, finer torn arrises and pits instead of big arrises are presented in Fig. 11d and e. However, there is also brittle failure with transgranular cleavage facets displayed in Fig. 11d and e, accordingly, the fracture surfaces in Fig. 11d and e are both quasi-cleavage fracture. From brittle to quasi-cleavage fracture, the production of IMCs Mg_2Ni, Mg_2Cu, and precipitated $Mg_{17}Al_{12}$ phase in

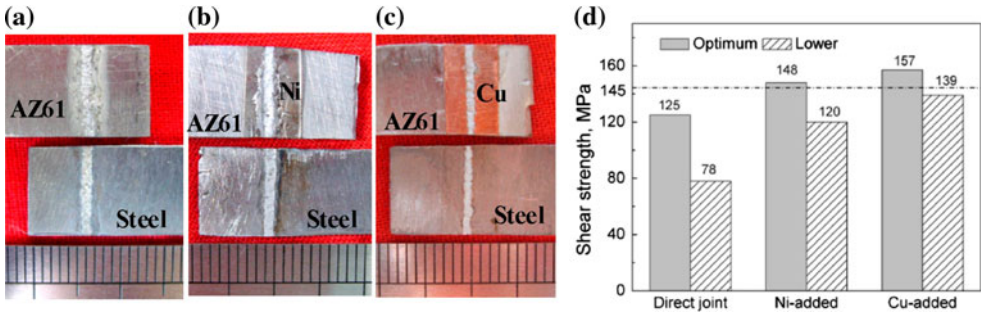

Fig. 10 Fracture location and shear strength of the joints with different interlayers: **a** direct joint, **b** Ni-added joint, **c** Cu-added joint, **d** shear strength of the joints with different interlayers. **a–c** were welded at optimum laser power. The lower joints in **d** were welded under the 380–390 W of laser power, which were all fractured like the pattern shown in (**a–c**)

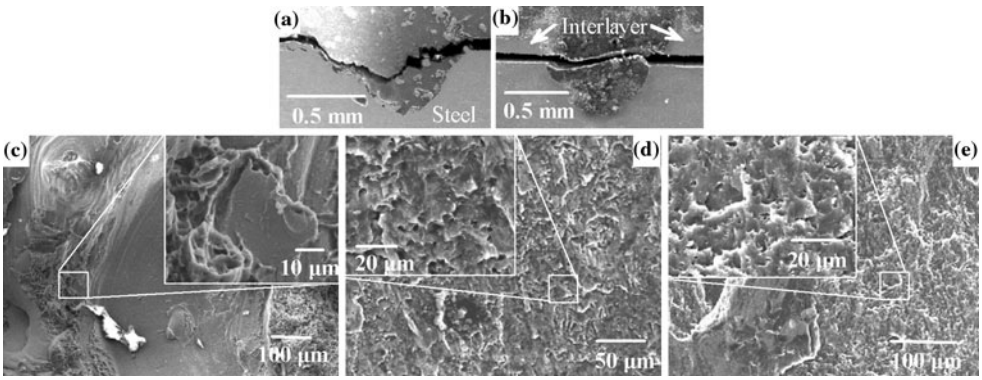

Fig. 11 Fracture mode of **a** direct joints and **b** interlayer-added joints; fracture surface of **c** direct joints, **d** Ni-added joints, and **e** Cu-added joints

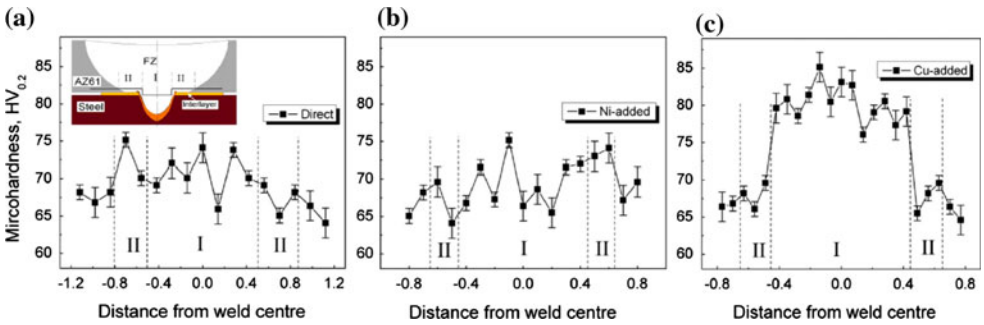

Fig. 12 Microhardness comparison of different joints: **a** direct joint, **b** Ni-added joint, **c** Cu-added joint

the FZ played an important role in strengthening effect. In addition, the profile of microhardness was performed in the FZ shown in Fig. 12. In the light of the fracture location and comparison with base material AZ61 Mg alloy, the indentations were carried out along the path shown in schematic view of a joint cross-section in Fig. 12a. It can be seen that the microhardness of Ni-added joint in the FZ is almost in the same level with that of direct joint, indicating that the effect of Mg_2Ni phase on joint strength is limited. Nonetheless, the hardness profile of Cu-added joint of Fig. 12c in the FZ is much higher than that of both Fig. 12a and b, furthermore, the strength of Cu-added joint is higher than that of Ni-added and direct joints shown in Fig. 10, consequently, it can be said that the intermetallic phases may be one of the reasons that strengthen the joints.

Discussion

AZ61 Mg alloy and Q235 steel sheets were lap joined by hybrid laser-TIG welding technique. One of the key factors that determined an effective joining is the joint tensile properties—tensile shear strength. Obviously, the shear strength of each sort of joints increases with the augment of penetration depth inside steel first and then decreases as shown in Fig. 2b. In the welding process, the penetration depth inside steel was determined mainly by the peak power of pulsed laser when all the other welding parameters were constant shown in Fig. 2a. Once the weld pool inside was created and when the welding process moved on, it would be filled with molten Mg alloy, thus the steel could hold the Mg alloy tightly after solidification. Therefore, the shear strength of the joint increased with the penetration depth inside the steel. However, further increasing the laser power, the joint shear strength was lowered. As the laser energy could melt steel during welding, the Mg alloy must be gasified drastically. Increasing laser power further indicates that much more Mg alloy would be gasified, consequently, the weld pool created inside steel could not be filled up in time, and holes would be formed in the weld after welding, which lowered the joint shear strength significantly. Besides, the joint shear strength is closely related to the bonding mode.

During solidification of direct joints, the wettability of molten Mg alloy on nucleating sites (solidified steel) is a crucial factor that decides the bonding strength [22, 23] owing to no interaction between Mg and Fe. The formation of gaps in Fig. 4b that deteriorates the bonding properties severely indicates that the wettability of AZ61 Mg alloy on steel plate is bad. However, the fact that the fracture mode shown in Fig. 11a displays that remnants of Mg alloy attached to the steel tightly could be ascribed partly to big difference of coefficient of thermal expansion (CTE) with 31.2×10^{-6}/K of AZ61 Mg alloy and 15×10^{-6}/K of Q235 steel. In the solidifying process the molten Mg alloy might hold the bulges which rose during welding, a compact bonding then could be obtained. What is more

important is that the microstructure and line analysis on the Mg alloy/steel interface of "Direct joint" section showed that no intermediate phases were found, thus the bonding mechanism of direct joint is mechanical joining.

When Ni or Cu interlayer was added into the joint, some changes occurred on the bonding mode of the joints. First, as for the Ni-added joints, a thin IMC layer which is Mg_2Ni phase connects the Ni interlayer with AZ61 Mg alloy at the Mg alloy/Ni interface shown in Fig. 4a. At the bottom of the pool, another layer of the TZ was formed shown in Fig. 3c. However, no Mg element was found in the TZ according to line analysis carried out along the line at the bottom shown in Fig. 5b. Therefore, the metallurgical bonding occurred between Mg alloy and Ni and between Ni and steel; while the bonding between Mg alloy and the TZ was still mechanical inside the pool. To sum up, the bonding mode of Ni-added joints is named "semi-metallurgical bonding".

Second, the bonding mode of Cu-added joints is identical with that of Ni-added joints. As Mg_2Cu is the landmark of metallurgical bonding between Mg alloy and Cu (see Fig. 8a and e), and limited solid solution of Cu in Fe (see Figs. 3e; 8c) in the TZ is another mark of metallurgical bonding between Cu and steel, whereas there is still no Mg element to be found in the TZ in terms of line analysis of Fig. 9b. From mechanical to semi-metallurgical bonding, the shear strength of joints achieves a great enhancement. As for the direct joint, Mg alloy and steel are bonded directly by the contact of the FZ with steel. While for the Ni- or Cu-added joint, the contact between Mg alloy and steel is constituted indirectly by the IMCs and the TZ. Consequently, during tensile shear test, not just the FZ of the joint but also these intermediaries which are IMCs and TZ could also bear the load, which enhanced the joint strength greatly, finally.

Nonetheless, it is notable that the difference among direct, Ni-added and Cu-added joints on microstructures of FZ shown separately in Figs. 4d, 5d, and 8d is distinct, which could also be seen from the fracture surface of Fig. 11. Instead of bigger torn arrises and larger smooth surface in the fractured FZ of direct joint in Fig. 11c, the fracture surface of interlayer-added joints is composed of uniform finer arrises and pits, indicating that the FZ of interlayer-added joints was refined. The crystals with white dots in Fig. 5d are finer than that in the direct joint of Fig. 4d; therefore, the FZ of Ni-added joint is strengthened, which is one of the reasons why the UTSS of Ni-added joint is higher than that of direct joint. However, the second phase Mg_2Cu with even finer stick structure also distributes discontinuously and uniformly in the grain boundaries of α-Mg in the FZ shown in Fig. 8d, consequently, the FZ of Cu-added joint is strengthened further, which might also be the reason that the UTSS of Cu-added joint is higher than that of Ni-added joint as the Fig. 10d shows.

Conclusions

AZ61 Mg alloy was successfully joined to Q235 mild steel by hybrid laser-TIG welding technique and the conclusions are as follows:

1. As mentioned above in "Discussion" section, the joint shear strength is related closely to the penetration depth, and increases with the augment of the depth.
2. Direct joint of AZ61 Mg alloy to Q235 mild steel is mechanical bonding; Ni- and Cu-added joints are semi-metallurgical bonding. Therefore, the joint shear strength could also be improved by the bonding mode transformation from mechanical to metallurgical.
3. The influence of Cu addition into the lap joint on the microstructures and shear strength is more relevant.

Acknowledgements The authors gratefully appreciate the sponsorship supported by National Natural Science Foundation of China (No. 50675028) and Supported by Research Fund for the Doctoral Program of Higher Education of China (No. 20070141031).

References

1. Cao X, Jahazi M, Immarigeon JP, Wallace W (2006) J Mater Process Technol 171:188
2. Su SF, Huang JC, Lin HK, Ho NJ (2002) Metal Mater Trans A 33A:1461
3. Shen J, You GQ, Long SY, Pan FS (2008) Mater Charact 59:1059
4. Liu LM, Dong CF (2006) Mater Lett 60:2194
5. Sathiya P, Aravindan S, Soundararajan R et al (2009) J Mater Sci 44:114. doi:10.1007/s10853-008-3098-8
6. Lu SP, Fujii H, Nogi K (2008) J Mater Sci 43:4583–4591. doi:10.1007/s10853-008-2681-3
7. Zhu JH, Li L, Liu Z (2005) Appl Surf Sci 247:300
8. Quan YJ, Chen ZH, Gong XS, Yu ZH (2008) Mater Charact 59:1491
9. Quan YJ, Chen ZH, Yu ZH, Gong XS, Li M (2008) Mater Charact 59:1799
10. Chi CT, Chao CG, Liu TF, Wang CC (2008) Vacuum 82:1177
11. Zhang B, Yuan SQ, Wang XH (2008) Rare Metals 27:393
12. Zhang H, Lin SB, Wu L, Feng JC, Ma Sh L (2006) Mater Des 27:805
13. Liu LM, Tan JH, Liu XJ (2007) Mater Lett 61:2373
14. Chen YC, Nakata K (2009) Mater Des 30:3913
15. Wielage B, Mucklich S, Grund T (2007) Microchim Acta 156:151
16. Liu LM, Qi XD, Wu ZH (2010) Mater Lett 64:89
17. Liu LM, Qi XD (2009) J Mater Sci 44:5725. doi:10.1007/s10853-009-3797-9
18. Amer AE, Koo MY, Lee KH et al (2010) J Mater Sci 45:1248. doi:10.1007/s10853-009-4074-7
19. Migiakis K, Papadimitriou GD (2009) J Mater Sci 44:6372. doi:10.1007/s10853-009-3878-9
20. Cao X, Rivaux B, Jahazi M et al (2009) J Mater Sci 44:4557. doi:10.1007/s10853-009-3691-5
21. Min D, Shen J, Lai SQ, Chen J (2009) Mater Charact 60:1583
22. Contreras A, Leon CA, Drew RAL, Bedolla E (2003) Scr Mater 48:1625
23. Hashim J, Looney L, Hashmi MSJ (2001) J Mater Process Technol 119:324